The universality class of percolation in doped ferroelasticity

Yunwei Mao*
Department of Mechanical Engineering,
Massachusetts Institute of Technology,
Cambridge, Massachusetts 02139, USA
(Dated: May 19, 2017)

The doping effects have been experimentally identified and theoretically studied in both ferromagnetic and ferroelectronic systems. The possible existence of similar effects in ferroelasticity is suggested by recent experiments; however, theoretically, it is still unclear what changes in ferroelastics with doped random fields, and whether the so-called glassy ferroelasticity is compatable with that in ferroelectronics and ferromagnetics. In this letter, we identify the class of universality of doepd ferroelastics, characterized by a set of critical exponents, through studying the morphologies and topologies of strain patterns in doped ferroelastics using a Laudau-Ginzburg model with suitable order parameters. The university class is the same with that of spin-glass, which demonstrating the similarity of doped effects in ferroelastics with that in ferromagnetics.

I. INTRODUCTION

The ferroic glasses [1], including relaxor ferroelectrics[2, 3], ferromagnetic cluster spin glasses[4], and the most recently proposed ferroelastic strain glasses[5], all have nanoscale heterogeneities in the ferroic order parameters (i.e., polarization, magnetization and strain, respectively). Typically, these ferroic glasses can be induced by introducing sufficient amount of random fields[2, 6]. In experiments, the random fields are usually introduced by doping point defects. As the doped defect concentration is low, normal first-order ferroic transition happens in the cooling process, and the low-temperature configurations are ferroic states with long-ranged order. As the doping concentration increases, these ferroic transitions would diffuse into second-order-like transition and the configurations at low temperature become the so-called ferroic glasses. It is believed that there exits a critical concentration of defects C_c. When the concentration of point defect, C, less than C_c, long-range-ordered ferroic states prevail at low temperature; otherwise, ferroic glass structure becomes predominant.

For relaxor and spin glass, nanostructures of ferroic states are usually embedded in high-temperature parent phase. For example, relaxor is thought to be a composite structure with nano-sized polar islands (several nanometers) in a cubic matrix of which the symmetry remains unchanged[2, 7]. Moreover, how the morphology changes from long-range-ordered ferroic state to ferroic glass is also researched. For instance, spin glass can be modeled using classic Ising model with random fields[8, 9]. When the concentration of point defects approaches C_c from the $C > C_c$ side, the isolated ferroic state islands would agglomerate and finally percolate at the critical concentration and ferroic state with long-ranged order appears.

For the recent proposed strain glass, it is also proved to be a composition of nano-sized martensite domains and surrouding matrix which has the same symmetry as that of autensite[10]. However, it remains unclear how the morphology and configuration change in doped ferroelasticity at low temperature along with defect concentration C. Moreover, whether the so-called glassy ferroelasticity is compatable with that in ferroelectronics and ferromagnetics is also unknown. In this letter, we analyzed the morphologies and topologies of strain patterns in doped ferroelastics using Laudau-Ginzburg model and identified its class of universality through critical exponents. The identified university class is the same with that of laser filamentation and spin-glass[11, 12], which demonstrating the similarity of doped effects in ferroelastics with that in ferromagnetics.

II. MODEL AND RESULTS

The details of our model is shown in previous papers[13, 14]. For completeness, we also described our model in details in the Appendix of this letter.

All the simulations are carried out in 2D with periodic boundary condition along two directions. The lattice we use to discretize the governing equation is 256×256. Larger sizes are tested and no essential differences are detected. All parameters setup is the same with that in our previous paper[14], except for the strength of random fields σ_J, which is 0.35 here. During the quench process, the temperature is decreased stepwisely by 1, and 20,000 steps are employed at each temperature to reach equilibrium. In order to sample different morphologies and configurations at the same doping level, over 1,000 tests were carried out with distinct defect distributions at each defect concentration.

Fig. 1 shows the statistics about the distribution of domain size $n_c(s)$ for samples with four different defect concentrations at a pre-set lowest temperature. Here s represents for the domain size. (a)-(d) are obtained at the following point defect concentrations: 0.000, 0.250, 0.350 and 0.450. The x-axis represents the size of do-

*Electronic address: yunweimao@gmail.com

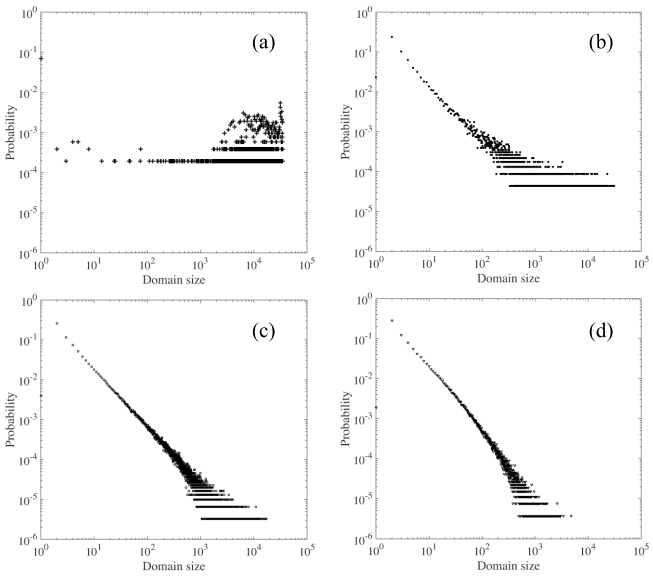

FIG. 1: The distribution of domain size $n_c(s)$ for samples under different point defects concentrations (0.000, 0.250, 0.350 and 0.450 for (a)-(d), respectively) at low temperature. The x-axis represents domain size s, and y-axis represents the frequency of domain size $n_c(s)$. For each concentration, at least 1,000 independent tests with different point defects distributions are analyzed.

mains, and y-axis represents the frequency of a certain domain size. The critical concentration is identified to be $C_c = 0.35$ (Fig.1 (c). The fat head for large domain size is from the finite size of simulation). When $C \ll C_c$, such as that displayed in (a), the typical size of martensite domains in the configuration is really large. As defect concentration increases, as shown in (b), a tail on the left of the figure appears, indicating that small domains are more likely to form rather than large domains, even though the final configuration is still martensite. The tail is "power-law" like and the whole curve looks like sub-critical state. As the concentration of point defects reaches the critical value $C_c = 0.35$, the distribution of domain size becomes perfectly power-law-like (see (c)). Continuingly increasing the concentration would make the power-law-like distribution in figure (c) becomes Γ distribution or super-critical distribution, which is characterized as a power-law for small domains but with an exponential tail for large ones.

In usual practice of percolation analysis, all critical exponents are defined through $|p-p_c|$[15, 16], where p is the filling factor, defined as the percentage of occupied sites by martensite within the entire lattice, and p_c is the filling factor when first percolation happened as p increases. In our simulations, we find that p_c is the filling factor at critical defect concentration, which is expected. In our following result section, most of the critical exponents are denoted as a function of $|C - C_c|$. So we first need to establish the relation between these two quantities. We

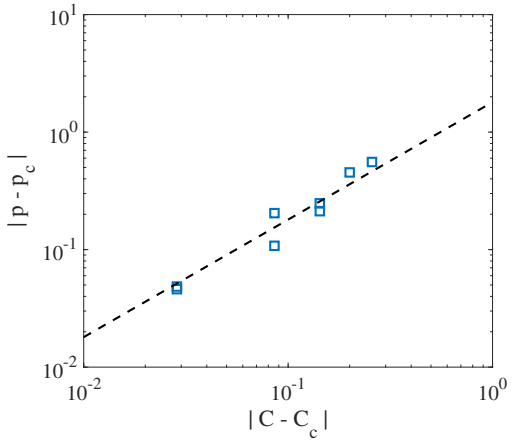

FIG. 2: Correlation between $|p - p_c|$ and $|C - C_c|$.

expect they are linearly dependent, since both of them can be the relevant direction,

$$|p - p_c| \sim |C - C_c|. \tag{1}$$

Indeed, this is supported by the fitting of the simulation data, as shown in Fig. 2, with identified critical values $C_c \approx 0.35$ and $p_c \approx 0.44$.

More information can be obtained by further analyzing Fig. 1. We first calculate the mean domain size S and the correlation length ξ versus $C - C_c$,

$$\begin{aligned} S &= \frac{\sum s^2 n_c(s)}{\sum s n_c(s)} \sim |C - C_c|^{-\gamma} \\ \xi^2 &= \frac{\int \mathrm{d}^2\mathbf{r} r^2 g(r)}{\int \mathrm{d}^2\mathbf{r} g(r)} \sim |C - C_c|^{-2\nu} \end{aligned} \tag{2}$$

where $g(r)$ is the probability that two martensite sites with a distance of r belong to the same domain. The best fit to the data gives $\gamma = 2.9$ and $\nu = 1.6$, which is displayed in Fig. 3.

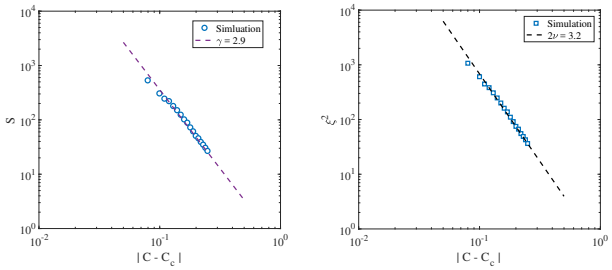

FIG. 3: Correlation of S and ξ^2 versus $|C - C_c|$.

In a finite system, ξ is bounded to the width L of the sampled squares. Near the criticality, it can therefore be assumed ξ linearly depends on L,

$$\xi \sim L \sim |C - C_c|^{-\nu} \tag{3}$$

so that the previous scalings can be rewritten as

$$S \sim L^{\gamma/\nu} \tag{4}$$

which gives $\gamma/\nu = 1.81$.

The exponents α, η can estimated through the hyperscaling relations:

$$\begin{aligned} \alpha &= 2 - d\nu \text{ (Josephson's identity)} \\ \eta &= 2 - \gamma/\nu \text{ (Widom's identity).} \end{aligned} \tag{5}$$

They lead to $\alpha = -1.2$ and $\eta = 0.18$.

We can obtain β from the definition

$$P_\infty = (C - C_c)^\beta \tag{6}$$

where P_∞ is the cluster strength, i.e., the probability that a site belongs to the percolating domain. Since we already estimate α and γ, we can estimate β from

$$\alpha + 2\beta + \gamma = 2 \text{ (Rushbrooke's relation)}, \tag{7}$$

which gives that $\beta = 0.15$. Then from Widom's identity, $\delta = 1 + \gamma/\beta$, we have $\delta \approx 20.3$. The error for δ is large, since β is pretty small.

As for the supercritical states, the distributions of domain size $n_c(s)$ can be fitted using following power law with exponential tail,

$$n_c(s) \sim s^{-\tau} \exp(-s/\mathcal{L}) \tag{8}$$

τ is the critical index and $\mathcal{L}$ is the cutoff domain size. This expression is also used to describe the domains size distribution in relaxor and spin glass[8,14], and can capture the experimental data very well. As shown in the Fig. 4(a), this expression also captures the trends of our simulation data. The fitting curve gives $\tau = 1.49$, and $\mathcal{L}$ varies with concentration sharply. The cutoff length is defined as $\ell_c = \sqrt{\mathcal{L}}$, which represents the characteristic cutoff length (since our simulation is in 2D). Fig. 5(b) highlights the variation of the correlation length with the doped defect concentration, diverges at $C_c = 0.35$, and then decreases sharply as the concentration increases. The insert figure shows the behavior of ℓ_c as a function of $C - C_c$, and the straight line indicates the common power law.

$$\ell_c = \sqrt{\mathcal{L}} \sim (C - C_c)^{-\zeta} \tag{9}$$

Here $\zeta = 1.5$ is another critical index. This critical index indicates that as the concentration approaches C_c, the nano-cluster martensite domains embedded in matrix will percolate (the connection graph will become simply- and path- connected, see Fig. 5), which makes the final configuration shift from nano-cluster martensite domains into martensite phase. So finally

$$n_c(s) \sim s^{-\tau} g_+((C - C_c)s^\sigma); \quad g_+(x) = \exp(-x^{1/\sigma}) \tag{10}$$

with $\tau = 1.49$ and $\sigma = 1/(2\zeta) = 0.33$.

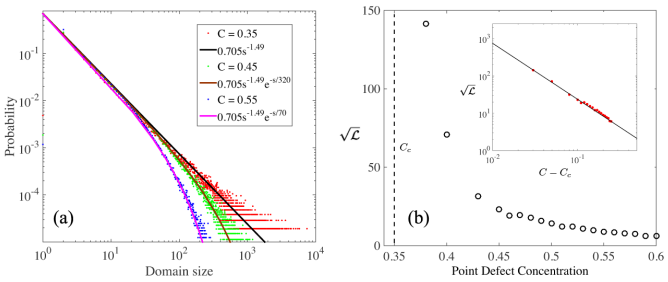

FIG. 4: Correlation length versus the point defect concentration. (a) Statistical results of the distribution of domain size of samples with defect concentrations 0.35, 0.45 and 0.55. The fit curves are also shown in this figure. (b) Statistical results of correlation length versus defect concentration. The same result displayed in bi-logarithm axes is shown in the insert panel.

TABLE I: Critical exponents in 2D ferroelastics simulations, and expected values for 2D uncorrelated percolation.

Critical exponent	Percolation in 2D-ferroelastics	2D-uncorrelated percolation
α	-1.2	-0.67
β	0.15	0.14
γ	2.9	2.34
δ	20.3	18.2
ν	1.6	1.33
η	0.18	0.21
σ	0.33	0.39
γ/ν	1.81	1.79
p_c	0.44	0.593

The critical exponents obtained from numerical simulation are summarized in Tab. I. Suprisingly, in contrast with the visual intuition from the similarity between percolation and the percolation in doped 2D ferroelastics, these values demonstrate that the martensite to strain glass due to doping does not belong to the same universality class with uncorrelated two dimensional percolation. But they are almost the same with those in laser filamentation[11]. Thus the laser filamentation, ferromagnetics[12], and ferroelastics share the same universality class.

There remains another problem. What happened at the critical point $C_c = 0.35$? More insights come from the relation between domains, i.e., the topological connection, as shown in Fig. 5. Fig. 5 (a)-(c) show the microscopic textures of three typical defect concentrations, 0.15, 0.35 and 0.55, respectively. These figures are colored by numbering of martensite domains, without distinguishing the type of variants of martensite phase. The lattice points in the same domain are rendered with the same color. (d)-(f) are abstracted from (a)-(c) and represent the topological connections between domains of the corresponding systems. In (d)-(f), a blue circle repre-

sents one single martensite domain. If two domains are neighbors, a pink line is used to link these two circles. When defect concentration is low (0.15 here), the system is filled with only a few (~ 10) large interconnected martensitic twinning domains (see Fig. 5(a)). The corresponding topology graph shown in Fig. 5(d) indicates that the ferroelastics at this doping level is simply- and path- connected. When the defect concentration is relatively large (0.55), the system is filled with thousands of nano-sized domains (see Fig. 5 (c)). Fig.5 (f) shows the corresponding topological connection. Since many domains in highly doped ferroelastics are isolated (isolated martensite islands surrounded by high-temperature parent phase), in order to make the connection clearly, those isolated islands are omitted. The graph in (f) is multiply- and non-path- connected. Two or three domains, embedded in the matrix, can connect with each other but cannot reach other domains.

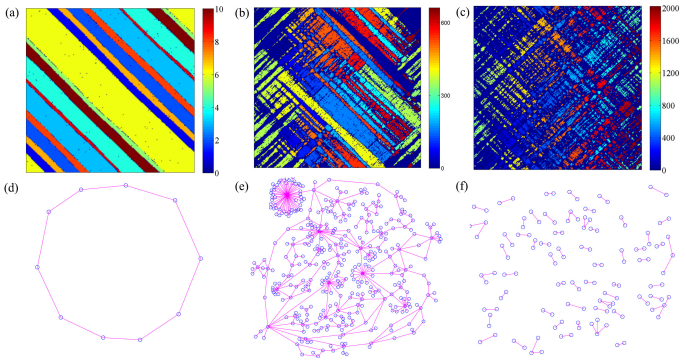

FIG. 5: The topological networking for samples with different concentrations of point defects at low temperature. (a)-(c) represent the microscopic texture of samples with point defect concentrations 0.15, 0.35, 0.55. Each color in the figures represents one domain. (d)-(f) The topological connections between domains. (d)-(f) are abstracted topologically from (a)-(c), respectively. A blue circle represents one domain. If two domains are neighbors, then a pink line is used to link these two circles.

When defect concentration is in between, particularly at the critical concentration 0.35, the domain distribution and the connection between the domains are shown in Fig.5 (b) and (e). There are typically hundreds of domains and the connection of these domains is different from both cases (0.15 and 0.55). On the one hand, it is different from the highly doped ferroelastics since domains are (nearly) simply- and path- connected. On the other hand, it is different from the 0.15 concentration case in several ways even though both are simply- and path- connected. The number of neighboring domains in low doping case is quite uniform, usually two; while in the intermediate doped ferroelastics, the number of neighboring domains varies from several to more than a dozen. Enlarging the simulation system will make the fluctuation even bigger. A very interesting result about the distribution of the connection number of domains within the system is shown in Fig. 6. The x-axis represents the number of neighbors one domain possesses, and y-axis represents the frequency $n(N)$. A power-law function

$$n(N) \sim N^{-3}, \tag{11}$$

where N is the number of neighbors a domain possessed, can be used to fit the simulation data very well. The same phenomenon is found in many fractals and complex network[17, 18]. This indicates the state with defect concentration 0.35 is a critical state, not only from the domain size distribution aspect with set of critical exponents, but also from the topology of the connectivity.

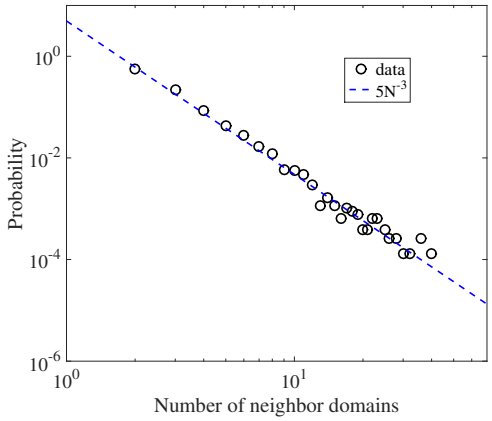

FIG. 6: The distribution of number of neighbors in topological connection graph. Only the case of the 0.35 defect concentration is shown. The x-axis represents the number of neighbors one domain possesses, and y-axis represents the frequency.

Considering the duality of the ferroelastic system is also interesting. For system without point defects, because of symmetry breaking as the temperature decreases, the martensite is the stable phase at low temperature while austenite is stable at high temperature. If we only focus on the low temperature phase, this can also be recast as following: for the case without random fields, the martensite is percolated at low temperature but austenite is not (see Fig 5(a) and (d)). As the concentration of point defects which generate random fields becomes very high, the martensite is not able to percolate through the system and austenite is percolated instead (Fig 5(c) and (f)). At the critical point C_c, both martensite and austenite are percolated through the system (Fig 5(b) and (e)). The competition between these two phases introduces the fractal structure at the critical point. Since the duality, p_c shall be around 0.5 for the martensite percolation and austenite percolation is a perfect duality. However, since the sites where the point defects sit prefer to stay in austenite phase even at low temperature, the perfect duality breaks. This induces $p_c < 0.5$.

III. DISCUSSIONS

We adopt the dissipative dynamics in this letter to obtain the low temperature structure states. A major concern is whether the states are equilibrium thermodynamics states. In simulations, the results essentially are the same with what we displayed here, with longer simulation time. However, how about the case with infinitely long simulation time? The short answer is that this concern is somewhat irrelevant to our topic. Shenoy et. al. [19] mapped the current continuum Landau-Ginzburg model to Blume-Emery-Griffiths spin-1/Potts model[20] with random strength of interactions, i.e.,

$$\beta\mathcal{H} = -\sum_{\langle i,j\rangle}\left[J_{ij}S_iS_j - \Delta(S_i^2+S_j^2) + KS_i^2S_j^2\right] \quad (12)$$

with $S_i = 0, \pm 1$, corresponding to austenite and two martensite variants. The defects induced by random field is introduced by setting randomness on J_{ij}, with mean J and variance σ_J.

By doing a position space renomalization group in a hierarchical lattice, Ozcelik et. al.[9] and Vasseur et. al.[21] demonstrates that in the spin-1/Potts model, there are three fixed points in the system at low temperature. $\sigma_J = 0$ and $\sigma_J = \infty$ are two stable fixed points and $\sigma_J = \sigma_J^\star > 0$ is unstable. If we map back to ferroelasticity system, then for $\sigma_J < \sigma_J^\star$, the final configuration is martensite, and for $\sigma_J > \sigma_J^\star$, the final configuration is another state, which has different order with martensite. This is clearly equivalent to change to C-direction, and the renormalization group tells there is an unstable fixed pointed C_c between two stable fixed points 0 and ∞.

Even though in spin-1 model, it is demonstrated that lower critical dimension d_ℓ for spin-glass phase lies somewhere between 2 and 3[9], and thus the spin-glass (then correspondingly glassy state in ferroelasticity) phase should be destroyed by thermal fluctuations in 2D, it essentially does not change our conclusion draw in this letter. To be precise, destroying the glassy phase in 2D does not mean destroying the fixed point $\sigma_J^\star$ or C_c; it only means $\sigma_J > \sigma_J^\star$ or $C > C_c$ cannot be interpreted as glassy phase. For example, in 2D ferroelasticity, only Tweed exists for $\sigma_J > \sigma_J^\star$ or $C > C_c$. Whether the case $\sigma_J > \sigma_J^\star$ is interpreted as tweed or glassy phase in ferroelasticity does not change the conclusion that we draw in this letter, since our conclusion on criticality does not depend on ergodicity of the "phase".

The next concern is about the reliability of the critical exponents displayed here, which are used to demonstrate the universality class of the doped ferroelasticity. We can check/improve the critical exponents that we obtained here by recalculating them using other methods. For example, for exponent ν we can also obtain it through percolation cumulant $\Pi(C, L)$[22],

$$\Pi(C, L) = \Phi((C - C_c)L^{1/\nu}) \quad (13)$$

for different sizes of L.

However, to eventually for complete the understanding of doped ferroelasticity with long-ranged interactions, extracting the critical exponents from renormalization group is very necessary. The analogy between the doped ferroelasticity and the spin-1 model with quenched disorders is not fully satisfied. We already see that the mapping relies on the assumption that the long-range elastic interaction displayed in the problem is not very relevant to the nature of the phases and transitions, which may not be true, especially for 2D. The reason is that the kernel for long-range elastic interaction $U(\mathbf{r}) \propto 1/r^2$, and thus the overall energy will look like $\sim \ln L$ in 2D, which needs greater attention.

IV. CONCLUSIONS

We recapitulated the information that we obtained from our model and numerical simulations. The morphology change in the doped ferroelastics can be treated as a critical phenomenon, from both the morphologies and topological connectivity of domains. We identified the critical exponents for the universality class of the doped ferroelasticity from numerical simulation of a Landau-Ginzburg model. The universality class of doped ferroelasticity is different from that of 2D uncorrelated percolation, but the same with laser filamentation and ferromagnetics. This highlights the deep connection among ferroelastics and ferromagetics.

V. ACKNOWLEDGEMENTS

I would like to thank Professor Mehran Kardar for a wonderful year in statistical physics, from particles to fields. It significantly broadens my sight and provides me some new ideas in research.

VI. APPENDIX: LANDAU-GINZBURG MODEL

In this section, without explicitly specifying, Einstein summation convention is used.

A generic cubic to tetragonal martensite transition is considered. In 2D, the configuration is transit from squared to rectangular. The two crystallographically equivalent and hence energetically degenerate Bain paths generate two deformation variants, which can be described by two non-conserved order parameter fields $\eta_1(\mathbf{r})$ and $\eta_2(\mathbf{r})$, respectively, in the Landau free energy, where $\mathbf{r}$ is the coordinate vector in 2D. Any given micro state in the system can be described by local values of these two order parameter fields. $(\eta_1, \eta_2) = (0, 0)$ represents the austenite and $(\eta_1, \eta_2) = (1, 0)$ or $(0, 1)$ represents one of the two deformation variants of the martensitic phase, respectively.

The eigenstrain, or the transformation strain, of the system is

$$\varepsilon^0_{ij}(\mathbf{r}) = \varepsilon^{00}_{ij}(1)\eta_1^2(\mathbf{r}) + \varepsilon^{00}_{ij}(2)\eta_2^2(\mathbf{r}), \tag{14}$$

with

$$\varepsilon^{00}_{ij}(1) = \varepsilon_0 \begin{bmatrix} 1 & 0 \\ 0 & -1 \end{bmatrix}; \quad \varepsilon^{00}_{ij}(2) = \varepsilon_0 \begin{bmatrix} -1 & 0 \\ 0 & 1 \end{bmatrix} \tag{15}$$

and ε_0 is the magnitude of the transformation strain.

The total free energy of the system F consists by two parts: the chemical free energy F_{chem} and the elastic strain energy E_{el},

$$F = F_{\text{chem}} + E_{\text{el}}. \tag{16}$$

The former one can be expressed as

$$F_{\text{chem}} = \int \mathrm{d}^2\mathbf{r} \left[\frac{1}{2}\beta(\nabla\eta_1)^2 + \frac{1}{2}\beta(\nabla\eta_2)^2 + f(\eta_1, \eta_2) \right] \tag{17}$$

with the first two terms in the blanket are the gradient energy terms with β for the interface energy. The last term is the local chemical free energy described with 6-order Landau polynominal

$$\begin{aligned} f(\eta_1, \eta_2) =& \frac{1}{2}A_1(\eta_1^2 + \eta_2^2) - \frac{1}{4}A_2(\eta_1^4 + \eta_2^4) \\ &+ \frac{1}{4}A_3(\eta_1^2 + \eta_2^2)^2 + \frac{1}{6}A_4(\eta_1^2 + \eta_2^2)^3 \end{aligned} \tag{18}$$

Here A_2 to A_4 are the expansion coefficients, and $A_1 = A_1^0(T - T_0)$ with T here is temperature and T_0 is the critical temperature for martensitic transition without any random fields. A_1^0 is also a expansion coefficient.The second part of the total energy, the elastic strain energy, is given by [23]

$$\begin{aligned} E_{\text{el}} =& \frac{1}{2}C_{ijkl}\varepsilon^{00}_{ij}(p)\varepsilon^{00}_{kl}(q) \int \mathrm{d}^2\mathbf{r}\eta_p^2(\mathbf{r})\eta_q^2(\mathbf{r}) \\ &- \frac{1}{2}\int \frac{\mathrm{d}^2\mathbf{k}}{(2\pi)^2} B_{pq}(\mathbf{e})\, \eta_p^2(\mathbf{k})\eta_q^2(-\mathbf{k}) \end{aligned} \tag{19}$$

with $B_{pq}(\mathbf{e}) = e_i c_{ijmn} C_{klrs} \Omega_{ik}(\mathbf{e}) \varepsilon^{00}_{mn}(p) \varepsilon^{00}_{rs}(q)$, $\mathbf{e} = \mathbf{k}/|\mathbf{k}|$. $\Omega_{ij}(\mathbf{e})$ is a Green function which is inverse of $\Omega^{-1}_{ij}(\mathbf{e}) = C_{iklj} e_k e_l$. Here C_{ijkl} is the 4-rank elastic constant tensor. For isotropic materials, only two independent constants are needed. Moreover, taking care that the symbols $\eta_p^2(\mathbf{k})$ and $\eta_p^2(\mathbf{r})$ are for

$$\eta_p^2(\mathbf{k}) = \int \mathrm{d}^2\mathbf{r}\eta_p^2(\mathbf{r}) e^{i\mathbf{k}\cdot\mathbf{r}}; \; \eta_p^2(\mathbf{r}) = \int \frac{\mathrm{d}^2\mathbf{k}}{(2\pi)^2} \eta_p^2(\mathbf{k}) e^{-i\mathbf{k}\cdot\mathbf{r}} \tag{20}$$

If the system is doped with point defects, whose role can be generalized as the global transition temperature effect, and local field effect, the local free energy (18) needs to be modified. Introduction of randomly distributed defects, in general, affects all four constants $A_1 - A_4$. However, since the constant A_1 plays an especially important role, we only modify it, and

$$\begin{aligned} f(\eta_1, \eta_2) =& \frac{1}{2}A_1'(\eta_1^2 + \eta_2^2) - \frac{1}{4}A_2(\eta_1^4 + \eta_2^4) \\ &+ \frac{1}{4}A_3(\eta_1^2 + \eta_2^2)^2 + \frac{1}{6}A_4(\eta_1^2 + \eta_2^2)^3 \\ &- \eta_{\text{loc}}(1)P(\eta_1, \eta_2) - \eta_{\text{loc}}(2)P(\eta_2, \eta_1) \end{aligned} \tag{21}$$

with $P(\eta_1, \eta_2)$ is a polynomial using to mimic the local field effect, which reads

$$\begin{aligned} P(\eta_1, \eta_2) =& A_1\eta_1 - \frac{1}{3}(A_2 - A_3)\eta_1^3 + A_3\eta_2^2\eta_1 \\ &+ \frac{1}{5}A_4\eta_1^5 + A_4\eta_2^4\eta_1 + \frac{2}{3}A_4\eta_2^2\eta_1^3 \end{aligned} \tag{22}$$

and $A_1' = A_1 + \sigma_J\bar{c}$, with σ_J is defect strength and $\bar{c}$ is the average defect concentration of the whole system.

The modification on $A_1 \to A_1'$ describes the global transition temperature effect, which is a mean-field effect. The $-\eta_{\text{loc}}(1)P(\eta_1, \eta_2) - \eta_{\text{loc}}(2)P(\eta_2, \eta_1)$ in (21) describe the local field effect, which are local random fields created by the point defects. The physical origin of the local field effect is lattice distortion caused by doped point defects, resulting in symmetry breaking of the Landau free energy.

The Landau-Ginzburg equation reads

$$\frac{\partial\eta_p}{\partial t} = -M\frac{\delta F}{\delta\eta_p} + \zeta(\mathbf{r}, t) \tag{23}$$

here $p = 1, 2$ and M is the mobility. $\zeta(\mathbf{r}, t)$ is used to mimic the thermal fluctuations, which is taken to be Gaussian distributed and its correlation properties meet the fluctuation-dissipation theorem:

$$\langle\zeta(\mathbf{r}, t)\zeta(\mathbf{r}', t')\rangle = 2k_BTM\delta(\mathbf{r} - \mathbf{r}')\delta(t - t') \tag{24}$$

[1] Peter Entel, Raymundo Arroyave, Sebastian Fähler, Ryosuke Kainuma, Antoni Planes, Xiaobing Ren, and Avadh Saxena. Ferroic glasses: Magnetic, polar and

strain glass. *physica status solidi (b)*, 251(10):1965–1966, 2014.

[2] Karin M Rabe, Charles H Ahn, and Jean-Marc Triscone. *Physics of ferroelectrics: a modern perspective*, volume 105. Springer Science & Business Media, 2007.

[3] L Eric Cross. Relaxor ferroelectrics. *Ferroelectrics*, 76(1):241–267, 1987.

[4] David Sherrington. A spin glass perspective on ferroic glasses. *physica status solidi (b)*, 251(10):1967–1981, 2014.

[5] Shampa Sarkar, Xiaobing Ren, and Kazuhiro Otsuka. Evidence for strain glass in the ferroelastic-martensitic system ti 50- x ni 50+ x. *Physical review letters*, 95(20):205702, 2005.

[6] Jian Zhang, Yu Wang, Xiangdong Ding, Zhen Zhang, Yumei Zhou, Xiaobing Ren, Dong Wang, Yuanchao Ji, Minghui Song, Kazuhiro Otsuka, et al. Spontaneous strain glass to martensite transition in a ti 50 ni 44.5 fe 5.5 strain glass. *Physical Review B*, 84(21):214201, 2011.

[7] Georgii Anatolevich Smolenskii. Physical phenomena in ferroelectrics with diffused phase transition. *J. Phys. Soc. Jpn*, 28(1):26–37, 1970.

[8] J Esser, Ulrich Nowak, and Klaus-Dieter Usadel. Exact ground-state properties of disordered ising systems. *Physical Review B*, 55(9):5866, 1997.

[9] V Ongun Özçelik and A Nihat Berker. Blume-emery-griffiths spin glass and inverted tricritical points. *Physical Review E*, 78(3):031104, 2008.

[10] Yumei Zhou, Dezhen Xue, Ya Tian, Xiangdong Ding, Shengwu Guo, Kazuhiro Otsuka, Jun Sun, and Xiaobing Ren. Direct evidence for local symmetry breaking during a strain glass transition. *Physical review letters*, 112(2):025701, 2014.

[11] Wahb Ettoumi, Jérôme Kasparian, and J-P Wolf. Laser filamentation as a new phase transition universality class. *Physical review letters*, 114(6):063903, 2015.

[12] Wahb Ettoumi, Jérôme Kasparian, and J-P Wolf. Spin-glass model governs laser multiple filamentation. *Physical review letters*, 115(3):033902, 2015.

[13] Dong Wang, Yunzhi Wang, Zhen Zhang, and Xiaobing Ren. Modeling abnormal strain states in ferroelastic systems: the role of point defects. *Physical review letters*, 105(20):205702, 2010.

[14] Junyan Zhang, Yunwei Mao, Dong Wang, Ju Li, and Yunzhi Wang. Accelerating ferroic ageing dynamics upon cooling. *NPG Asia Materials*, 8(10):e319, 2016.

[15] H Eugene Stanley. Scaling, universality, and renormalization: Three pillars of modern critical phenomena. *Reviews of modern physics*, 71(2):S358, 1999.

[16] Santo Fortunato and Helmut Satz. Cluster percolation and pseudocritical behaviour in spin models. *Physics Letters B*, 509(1):189–195, 2001.

[17] R Orbach. Dynamics of fractal networks. *Science*, 231:814–820, 1986.

[18] Albert-László Barabási and Réka Albert. Emergence of scaling in random networks. *science*, 286(5439):509–512, 1999.

[19] SR Shenoy and T Lookman. Strain pseudospins with power-law interactions: Glassy textures of a cooled coupled-map lattice. *Physical Review B*, 78(14):144103, 2008.

[20] M Blume, VJ Emery, and Robert B Griffiths. Ising model for the λ transition and phase separation in he 3-he 4 mixtures. *Physical review A*, 4(3):1071, 1971.

[21] R Vasseur, D Xue, Y Zhou, W Ettoumi, X Ding, X Ren, and T Lookman. Phase diagram of ferroelastic systems in the presence of disorder: Analytical model and experimental verification. *Physical Review B*, 86(18):184103, 2012.

[22] K. Binder and D.W. Heermann. *Monte Carlo simulations in statistical physics, An introduction*. Springer Science & Business Media, 1988.

[23] Armen G Khachaturyan. *Theory of structural transformations in solids*. Courier Corporation, 2013.